ADVANCED MATERIALS
www.advmat.de

Highly Thermotolerant Metal Halide Perovskite Solids

Huiwang Lian, Yang Li, Kaniyarakkal Sharafudeen, Weiren Zhao, Gopi R. Krishnan, Shaoan Zhang, Jianrong Qiu,* Kai Huang, and Gang Han**

By virtue of their narrow emission bands, near-unity quantum yield, and low fabrication cost, metal halide perovskites hold great promise in numerous aspects of optoelectronic applications, including solid-state lighting, lasing, and displays. Despite such promise, the poor temperature tolerance and suboptimal quantum yield of the existing metal halide perovskites in their solid state have severely limited their practical applications. Here, a straightforward heterogeneous interfacial method to develop superior thermotolerant and highly emissive solid-state metal halide perovskites is reported and their use as long-lasting high-temperature and high-input-power durable solid-state light-emitting diodes is illustrated. It is found that the resultant materials can well maintain their superior quantum efficiency after heating at a temperature over 150 °C for up to 22 h. A white light-emitting diode (w-LED) constructed from the metal halide perovskite solid exhibits superior temperature sustainable lifetime over 1100 h. The w-LED also displays a highly durable high-power-driving capability, and its working current can go up to 300 mA. It is believed that such highly thermotolerant metal halide perovskites will unleash the possibility of a wide variety of high-power and high-temperature solid-state lighting, lasing, and display devices that have been limited by existing methods.

Metal halide perovskites (i.e., $CsPbX_3$, X = Cl, Br, and I) have emerged as one of the most promising materials for a variety of optoelectronic applications, such as light-emitting diodes,[1] photodetectors,[2] solar cells,[3] lasers,[4] and solid-state lighting.[5] This is due to their unique properties, such as their near-unity photoluminescence quantum efficiency (PLQY),[6] narrow-band emission (full width at half maximum, FWHM, ≈20 nm),[7] tunable emission, low fabrication cost, and scalability.[8] Despite such promise, rapid luminescence quenching in their solid state and poor temperature tolerance of the existing solid-state perovskites have severely impeded their practical optoelectronic applications, especially those requiring prolonged operations. In particular, the PLQY of perovskites collapse sharply when perovskites are extracted from the organic solution to form a bulk-solid in regard to solid-state device fabrication.[9] This problem becomes particularly severe when the operation temperature increases to 100 °C,[10] leading to significant challenges for these lighting, lasing and display applications whose operation is associated with high thermal or high power conditions.

Here, we propose and report on a straightforward heterogeneous interfacial thermal (HIT) strategy to develop highly thermotolerant metal halide perovskite solids (HPSs) (**Figure 1**a). The generated highly thermotolerant (HT) $CsPbBr_3$/Cs_4PbBr_6 halide perovskite solid-powders (HT-HPSs) exhibit a maximum PLQY of 95% when being suspended in organic solvent. After they are extracted from the solution, the PLQY of these solids can still well remain at 84% at room temperature, and 73% after heat acclimation at 150 °C for up to 22 h. Such unprecedent outstanding properties with respect to HT-HPSs are essential to address the abovementioned poor temperature tolerance and low PLQYs of perovskite solids regarding their optoelectronic applications. To illustrate such applications, we constructed a white light-emitting diode (w-LED) using our optimal HT-HPSs. Compared to commercial w-LED, our w-LED

Dr. H. Lian, Prof. Y. Li, Prof. W. Zhao
School of Physics and Optoelectronic Engineering
Guangdong University of Technology
Guangzhou 510006, China
E-mail: lychris@sina.com
Prof. K. Sharafudeen
Kuwait College Science and Technology
Doha 27335, Kuwait
Dr. G. R. Krishnan
Department of Physics
NSS College Pandalam
Pathanamthitta, Kerala 689501, India
The ORCID identification number(s) for the author(s) of this article can be found under https://doi.org/10.1002/adma.202002495.
Prof. S. Zhang
School of Optoelectronic Engineering
Guangdong Polytechnic Normal University
Guangzhou 510665, China
Prof. J. Qiu
State Key Laboratory of Modern Optical Instrumentation
College of Optical Science and Engineering
Zhejiang University
Hangzhou, Zhejiang 310058, China
E-mail: qjr@zju.edu.cn
Dr. K. Huang, Prof. G. Han
Department of Biochemistry and Molecular Pharmacology
University of Massachusetts Medical School
Worcester, MA 01605, USA
E-mail: Ganghan@umassmed.edu

DOI: 10.1002/adma.202002495

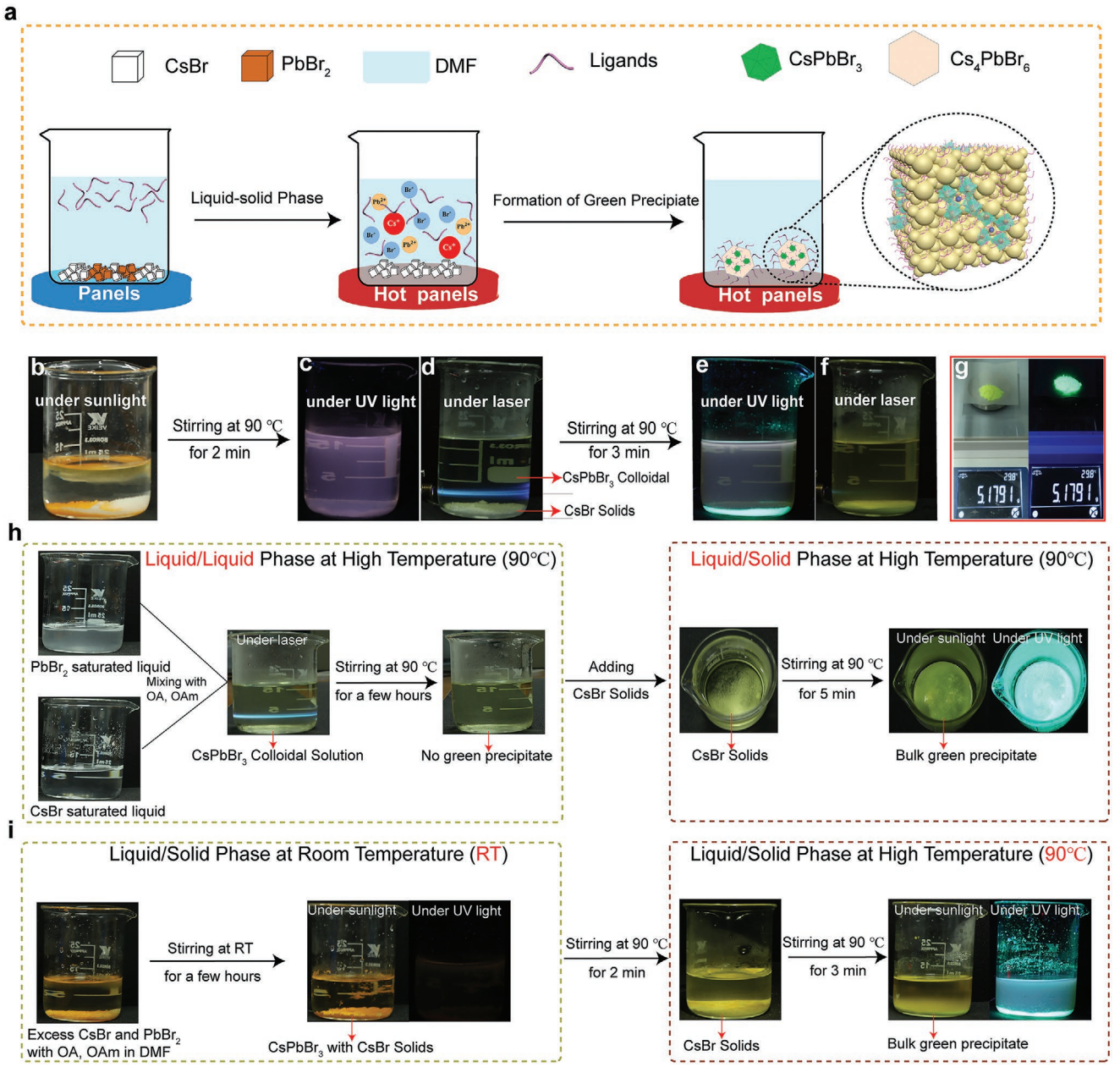

Figure 1. Liquid/solid heterogeneous interfacial thermal (HIT) reaction for synthesizing HT-HPSs. a) Schematic illustration of HIT evolution between the immiscible liquid–solid phases at 90 °C. b) Photographs showing no colloidal phase formed at room temperature. c,d) Photographs showing the $CsPbBr_3$ colloidal phase formed at 90 °C in the first 2 min of the reaction. e) Photographs showing the instantaneous appearance of $CsPbBr_3$/Cs_4PbBr_6 green precipitates. f) Photographs showing no colloidal phase existed after the reaction. g) Nearly quantitative reaction yield for large-scale production. h) Photographs of the liquid/liquid phase and liquid/solid phase reactions at high temperature, showing that the liquid–solid phase was essential to promote the reaction. i) Photographs of liquid/solid phase reaction at room temperature and high temperature, showing that high temperature was indispensable for the formation of $CsPbBr_3$ colloidal liquid.

shows advantages with respect to narrow emission (FWHM ≈ 20), high color purity, and wider color gamut. More importantly, such w-LED also possesses outstanding long-term thermal stability and its lifetime can last over 1100 h, which is three orders of magnitude longer compared to a standard conventional synthesized $CsPbBr_3$ constructed LED. This can even be comparable to the durability of the commercial w-LED. Moreover, our w-LED also displays a superior durable high-power-driving capability, and its working current can go up to 300 mA, which is much higher than any previously reported materials (200 mA is the highest reported in the literature[11]).

In this study, rather than currently used liquid/liquid reaction which occurs in homogeneous solution phases,[8] we developed a heterogeneous liquid/solid phase interfacial thermal (HIT) reaction to synthesizes metal halide perovskite solids (Figure 1a). In our reaction, $PbBr_2$ and excess CsBr, along

with oleic acid (OA) and oleylamine (OAm), were sequentially dissolved in DMF, and reddish precipitation immediately appeared (Figure 1b). This reddish solid was identified to be $CsPbBr_3$ by the XRD patterns (Figure S1, Supporting Information). After further stirring for 2 min at 90 °C, due to the high solubility of $CsPbBr_3$ at such temperature, the $CsPbBr_3$ began to be dissolved and excess white CsBr still existed.[12] At this step, nearly no luminescence was observed under excitation by 365 nm light (Figure 1c). Under the irradiation with a 405 nm laser, the transparent solution exhibited a distinct Tyndall effect, indicating the formation of $CsPbBr_3$ colloids (Figure 1d). After stirring for another 3 min, a homogeneous and intense green luminescence emerged instantaneously, and then green solid precipitated at the bottom of the reaction beaker (Figure 1e). The supernatant solution exhibited no Tyndall effect (Figure 1f), suggesting that nearly all the $CsPbBr_3$ colloidal in the solution reacted with excess CsBr to produce green-emitting perovskite solids. Our HIT reaction is highly effective, and the highest product yield is up to 99%. This reaction can also be readily scaled up and over 5 g of the products can be synthesized at one time without compromised PLQY (Figure 1g).

Next, we studied two key experimental factors in the formation of the green-emitting perovskite solids. The first consideration is the necessary of using a liquid–solid solution phase in our reaction. In the liquid–liquid phase reaction, even the saturated solution of CsBr was dropped into the saturated solution of $PbBr_2$, still no green precipitates were generated in such a homogeneous phase system even after stirring for dozens of hours at 90 °C (Figure 1h). In contrast, by adding excess CsBr solids at that stage, bulk green products appeared immediately. Therefore, the heterogeneous liquid/solid interfacial reaction is the precondition for successfully fabricating perovskite solids. The second consideration is the temperature dependence for HIT reaction. If the proposed reaction occurred at room temperature, only nonluminescent reddish $CsPbBr_3$ precipitates were generated (Figure 1i). In contrast, when the reaction temperature increased to 90 °C, the reddish $CsPbBr_3$ solids were gradually dissolved in solution and transformed into colloids. The supernatant after HIT reaction subsequently lose the complete transparence, and the precipitates showed green luminescence under ultraviolet (UV) light. Seemingly, high temperature facilitates the heterogeneous phase reactions between immiscible $CsPbBr_3$ colloids and CsBr solids.

Following the above HIT evolution, we fabricated green-emitting HT-HPSs with uniform morphology (**Figure 2**d). These green precipitates were verified to be assembly of hybrid structured particles where $CsPbBr_3$ perovskites were embedded into Cs_4PbBr_6 hosts based on XRD measurement (Figure 2b). When the $CsBr/PbBr_2$ molar ratio was 1:1, the X-ray diffraction (XRD) patterns of the solids showed only the characteristic peaks of pure $CsPbBr_3$ perovskites. As the Cs^+ concentration increased, new XRD peaks gradually appeared at $2\theta = 12.9°$, 20.1°, 22.4°, corresponding to diffractions from the (110), (113), and (300) planes of rhombohedral Cs_4PbBr_6 (PDF card#73-2478). These results all implied the formation of the $CsPbBr_3/Cs_4PbBr_6$ structure. This hybrid structure was also confirmed by UV–vis spectroscopy (Figure S2, Supporting Information). These obtained HT-HPSs with $CsPbBr_3/Cs_4PbBr_6$ structure showed a color gradient of reddish-to-yellow (Figure 2a). Under the irradiation of 365 nm UV light, all $CsPbBr_3/Cs_4PbBr_6$ HT-HPSs exhibited a narrow-emissive (the full width at half maximum is 20 nm) green luminescence at 520 nm (Figure 2c). As the Cs^+ concentration increased, the brightness of the green emission gradually increased, reaching a maximum at a $CsBr/PbBr_2$ molar ratio of 6:1 (Figure 2a). When monitoring 520 nm emission, the photoluminescence excitation spectra revealed two broad excitation bands peaking at 291 and 352 nm, which well match the excitation bands of previously reported $CsPbBr_3/Cs_4PbBr_6$ perovskites (detailed discussions in Figure S3 of the Supporting Information).[12,13]

To further demonstrate the superiority on high emission, the PLQYs of all HT-HPSs were measured and showed in Figure 2e. The HT-HPSs synthesized with $CsBr/PbBr_2$ molar ratios of 1, 2, 3, 4, 6, 8, 10, and 12 were 2.1%, 29.65%, 49.23%, 50.78%, 84%, 68.75%, 65.47%, and 52.12%, respectively (Figure S4, Supporting Information). When the strongest emissive HT-HPSs with $CsBr/PbBr_2$ molar ratio of 6:1 (called HT-HPSs-6) were suspended in a mixed solution of cyclohexane and isopropanol, their PLQY was even greater than 94%, which is comparable to the reported maximum PLQY of green-emissive quantum dots dissolved in solution. Moreover, our HT-HPSs can also endure high-intensity purification tolerance, which is one of the important indexes of evaluating the synthesis reproducibility and optical performance (Figure S5, Supporting Information). More notably, even after nine purification cycles of dissolution-to-centrifugation, the solutions and solids still emitted strong green luminescence and their PLQYs remained above 93% and 75%, respectively (Figure 2f). These results suggest that our HT-HPSs synthesized by HIT reaction have strong emission not only in their solution suspension but also in their solid state, and optimal HT-HPSs-6 shows significant purification tolerance superior to the existing perovskites.[14]

We further proposed the possible origination of high PLQYs of our HT-HPSs. First, The structural encapsulation of Cs_4PbBr_6 to $CsPbBr_3$ perovskites are considered to be an effective passivation strategy for enhancing the green luminescence of $CsPbBr_3$, since the spatial confinement of Cs_4PbBr_6 strongly enhances the radiative rate of the $CsPbBr_3$.[15] In Figure 2e, the PLQY of the most used standard perovskite solid ($CsPbBr_3$ solid) is only 0.8%, yet the PLQY of HT-HPSs-6 increased nearly 800-fold in comparison with such pure $CsPbBr_3$ solid. Second, in addition to the hybrid structure, the surface ligand modification is also considered to be beneficial to the highly emissive properties of HPSs.[16] The surface ligands can effectively suppress the generation of surface defects and impeded charge recombination of the inner the defects.[1g,17] In particular, as a control, the ligand-free $CsPbBr_3/Cs_4PbBr_6$ halide perovskite solids were prepared via the same reaction without OA and OAm. However, the maximum PLQY of these HPSs with $CsBr/PbBr_2$ molar ratios of 6:1 was only 48.72% in their solid state, which was much smaller than the PLQY of HT-HPSs-6 (Figure S6, Supporting Information and Figure 2e). Moreover, due to the absence of surface ligands, these ligand-free HPSs control samples were insoluble in cyclohexane and isopropanol solution (Figure S7, Supporting Information). Therefore, the hybrid $CsPbBr_3/Cs_4PbBr_6$ structure and surface ligand are considered to ensure the high PLQY for our HT-HPSs-6.

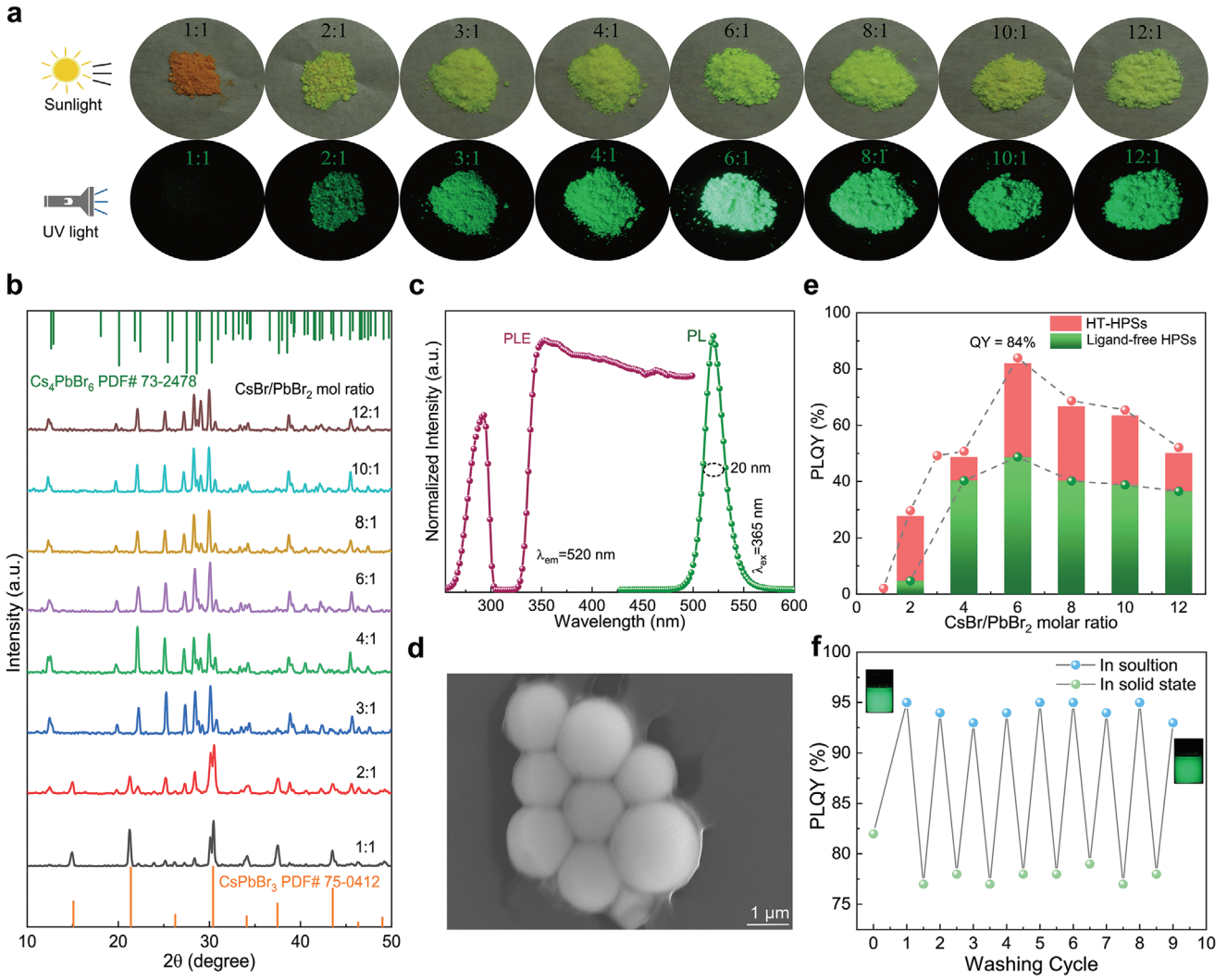

Figure 2. Optical properties, morphology, and structure phase. a) Photographs of HT-HPSs under sunlight and UV irradiation. b) XRD patterns of HT-HPSs formed with different $CsBr/PbBr_2$ molar ratios. c) Normalized photoluminescence (excited by 365 nm), photoluminescence excitation (monitored at 520 nm) spectra. d) SEM of HT-HPSs-6. e) PLQYs of HT-HPSs and ligand-free HPSs with the $CsBr/PbBr_2$ molar ratios of 1, 2, 3, 4, 6, 8, 10, and 12, respectively. f) PLQYs of HT-HPSs-6 in solution and the solid-state after 1–9 cycles of washing.

Besides such high PLQYs and purification durability, our HT-HPSs are also conferred unprecedentedly excellent chemical stability and thermotolerance, which are crucial to meet the requirements of practical lighting application. Our HT-HPSs showed stable light emission, with minimal degradation after eleven weeks of storage under ambient condition (Figure S8, Supporting Information). Temperature-dependent PLQY data and color images were obtained at ambient temperature after heating at different temperatures (**Figure 3**a). After heating at 200 °C for 1 h, HT-HPSs-6 still possessed the maximum green emission (Figure S9, Supporting Information). The panda images made by our optimal HT-HPSs-6 ($CsBr/PbBr_2$ molar ratio of 6:1) exhibited high PLQYs of 84%, 78%, 73%, 65% after heating at 30, 100, 150, 200 °C, respectively. The green luminescence only starts to drop at 250 °C (Figure S10, Supporting Information). Even after ten consecutive heating–cooling cycles over the temperature ranges of 30–200 °C, there was still no decrease in the intensity during cycling (Figure 3d). In addition, time-dependent intensity stability under heat treatment at 150 °C further verified the satisfactorily thermotolerance, since green luminescence in the shape of a small phoenix logo made by our HT-HPSs-6 under excitation at 365 nm remained nearly unchanged even after 22 h of heat treatment (Figure 3b,c).

More notably, the ambient beyond 200 °C did not alter the structural framework of HT-HPSs, since no obvious variation in XRD patterns was found in the temperature-dependent XRD measurement after returning to room temperature from the treatment point (Figure 3e). Even when the ambient temperature exceeds 300 °C, the surface ligands of our material have hardly changed (Figure 3f).

These results all suggest that our HT-HPSs have the more superior thermotolerance than those other reported materials, and such thermotolerance is considered to be related with their structure frameworks and surface ligands. First, since

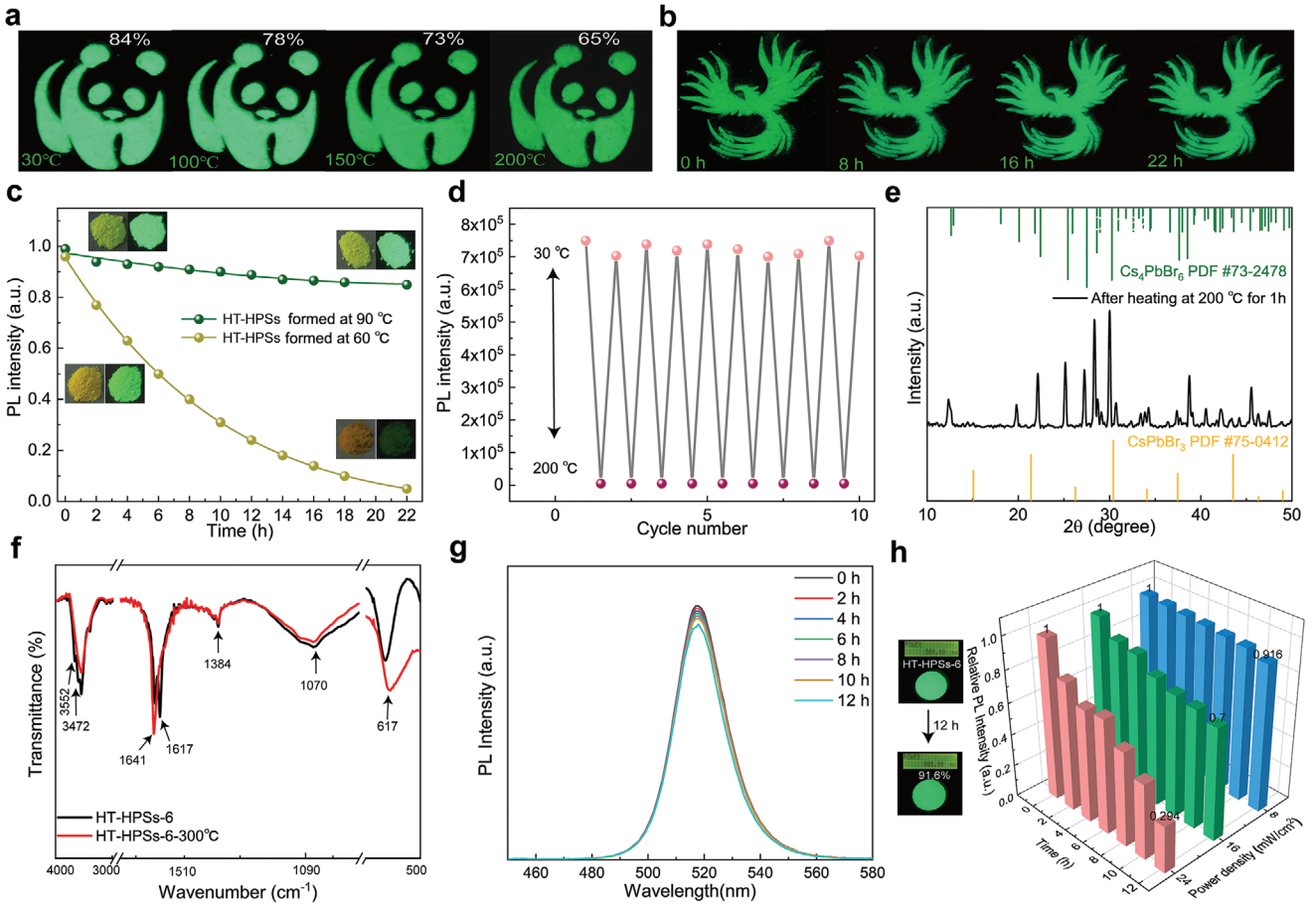

Figure 3. Thermotolerance and UV photostability. a) FLuorescence photographs and PLQY of HT-HPSs-6 at ambient temperature after heat treatment (30–200 °C) for half an hour. b) Fluorescence photographs and c) time-dependent intensity stability after heating at 150 °C for various times ranging from 0 to 22 h. d) The reversible fluorescence response of 10 consecutive cycles at 30–200 °C. e) XRD pattern of HT-HPSs-6 after heating at 200 °C for 1 h. f) FTIR spectra of HT-HPSs-6 at room temperature (black) and after heating at 300 °C (red) for 1 h. g) The PL spectra of HT-HPSs-6 under continuous illumination by 365 nm light, the power density is 8 mW cm^{-2}. h) Fluorescence photographs of HT-HPSs-6 under UV light with a power density of 8 mW cm^{-2} for 12 h (left); HT-HPS-6 under continuous illumination with 365 nm light (right); the power densities are 8, 16, and 24 mW cm^{-2}, respectively.

the large binding energy (>303.9 meV) of $PbBr_6^{4-}$ octahedron in Cs_4PbBr_6 strongly enhances the lattice stability, the Cs_4PbBr_6 has superior structure stability compared to $CsPbBr_3$. Thus, the hybrid encapsulation structure of Cs_4PbBr_6 to $CsPbBr_3$ is beneficial for the boosted thermotolerance.[18] In a contrasting experiment, lower-thermotolerant (LT) HPSs at $CsBr/PbBr_2$ molar ratio of 6:1 (LT-HPSs-6) were formed at a lower temperature (60 °C), and such low synthesis temperature observably suppressed the transformation of $CsPbBr_3$ to Cs_4PbBr_6 in our reaction (Figure S11, Supporting Information). As shown in Figure S11 (Supporting Information), the normalized absorption spectra of HT-HPSs-6 (materials synthesized at 90 °C) and LT-HPSs-6 (materials synthesized at 60 °C) are present. At the absorption band of 520 nm, which is assigned to the inter-transition of $CsPbBr_3$, LT-HPSs-6 showed a stronger absorption ability than HT-HPSs-6, implying that the percentage of $CsPbBr_3$ in LT-HPSs-6 is at a higher level in comparison with HT-HPSs-6. It should be mentioned that the synthesis of LT-HPSs-6 at 60 °C requires a reaction time beyond 60 min (Figure S12, Supporting Information), which is clearly longer than that of the thermotolerant HT-HPSs-6. However, even with this longer reaction time, such low-efficient transformation from $CsPbBr_3$ to Cs_4PbBr_6 at 60 °C leads to the appearance of low PLQY (28.03% for LT-HPSs-6) and poor thermotolerance of LT-HPSs-6 (Figure 3c).

Secondly, the excellent thermotolerance can also be related with surface ligands. On the one hand, similar to LT-HPSs-6 and HPSs synthesized by the conventionally utilized hot-injection and supersaturation precipitates methods, typical vibrations (3400–3600, 2800–3000, ≈1600, ≈1463, and ≈716 cm^{-1}) belonging to OA and OAm (Figure S13 and Tables S1 and S2, Supporting Information) are also present on the surface of our thermotolerant material, HT-HPSs-6;[16–18] on the other hand, the Fourier transform infrared (FTIR) spectrum of our HT-HPSs-6 exhibits additional vibrations that are not observed in the FTIR spectra of the LT-HPSs-6 and other materials synthesized by existing methods. The two additional strong vibrations at 1641 and 617 cm^{-1} on the FTIR spectra of HT-HPSs-6 can be ascribed to C=O stretching vibration and the O—C—N bending of DMF, respectively (Figure 3f and Table S1, Supporting

Information).[19,20] Therefore, based on the FTIR results, in addition to the presence of OA and OAm, solvent DMF molecules are also suggested to be binding to the surface of our thermotolerant material.

As shown in Figure 3f and Figure S13 (Supporting Information), to evaluate the thermal stability, we heated both HT-HPSs-6 and LT-HPSs-for 1 h at 300 °C . After this treatment, there was almost no decrease in intensity appeared in the FTIR spectra of HT-HPSs-6, while the intensity of all FTIR peaks of LT-HPSs-6 significantly decreased. The thermogravimetric (TG) result (Figure S14, Supporting Information) also supports the fact that LT-HPSs-6 has poor thermotolerance, and that the ligands on the surface of LT-HPSs-6 began to be decomposed at 100 °C, while the weight loss of HT-HPSs-6 is negligible, even beyond 300 °C. Therefore, we consider that both DMF ligand and Cs_4PbBr_6 hybrid encapsulation contributed to the enhanced the perovskite stability against high temperatures.

Ultraviolet (UV) photostability is another important parameter that determines the long-term operation of perovskite-based lighting devices. The PL intensity at 520 nm emission of HT-HPSs-6 showed no noticeable decrease after the irradiation of continuous UV light with an optical power density of 8 mW cm^{-2} for 12 h (Figure 3g), while LT-HPSs-6 only maintained 25% luminescence intensity at the same measurement conditions (Figure S15, Supporting Information). The strong UV photostability is likely due to stable Cs_4PbBr_6 encapsulation, since this framework is known to be resistant against UV deterioration;[5b] actually, the green luminescence of the bare $CsPbBr_3$ solid only can last less than 1 h under the irradiation at 365 nm light. When the power density of ultraviolet light was increased to 16 and 24 mW cm^{-2}, respectively, the HT-HPSs-6 decreased to 70% and 29.4% of its initial value under continuous UV light for 12 h (Figure 3h). Such UV photostability of our HT-HPSs-6 is superior to the existing perovskite powders, since the existing materials almost lose their luminescence under UV irradiation with an optical power density of 24 mW cm^{-2}.[8a,10a] In fact, the working power of conventional lighting devices is 8 mW cm^{-2}, and the power density of 24 mW cm^{-2} is beyond that.[21] All the results indicate that our HT-HPSs-6 have the potential applied as optical converters in harsh conditions than the previous solid-state perovskites.

On basis of the promise of high thermotolerance and photostability, we went on to fabricate a white-LED using our HT-HPSs-6 as the green conversion hub in addition to $Y_2O_3:Eu^{3+}$ (red converter), and $BaMgAl_{10}O_{17}:Eu^{2+}$ (blue phosphor) which have been using on a commercial LED chip. **Figure 4**a presents the electroluminescence (EL) spectra obtained at a current density of 20 mA, which is the typical operating current for LEDs regarding their use in ambient condition. The working white-light LED shows neutral white light with a color rendering index (CRI) of 86.1, a correlated color temperature (CCT) of 4843 K, and Commission Internationale de l'Eclairage (CIE) coordinates of (0.3448, 0.3131). Moreover, the color gamut of the white LED, as presented in Figure 4b (thick solid triangle), covers 116.3% of the NTSC (dotted triangle) gamut and 86.2% of the Rec. 2020 gamut (dashed triangle). In addition, w-LED-based HT-HPSs-6 operating at 20 mA still maintain very high luminescence intensity (more than 90% of initial value) for 1100 h (Figure 4c), while the luminescence intensity of the pure $CsPbBr_3$ solid quickly diminished in less than 2 h. The low luminous decay and superior long lifetime is ideal for practical commercial application purposes. Figure 4e,f shows pictures of the device and illustrates the long-term operation stability. Moreover, the existing commercial white-light source is composed by a semiconductor GaN-based chip coated with rare-earth-doped phosphors, such as green-emitting $Ce:(Lu_xY_{1-x})_3Al_5O_{12}$ (Ce:Lu-YAG) and β-SiAlON: Eu^{2+} phosphors, and red-emitting K_2SiF_6: Mn^{4+} phosphors.[22] Although this schema generates high-quality white light at a low cost, its color gamut is not satisfactory. This is attributed to the suboptimal bandwidth of green-emitting phosphors (FWHM > 50 nm) prominently suppresses visual luminous efficacy and color resolution.[23] Here, our HT-HPSs-6 show a significantly narrower FWHM (≈20 nm) than commercially available $Ce:(Lu_xY_{1-x})_3Al_5O_{12}$ (Ce:Lu-YAG) (FWHM of 92 nm) phosphors (Figure S16, Supporting Information). Therefore, the narrow FWHM enables our materials to possess the potential for the application in wide color-gamut backlight display.

In addition to the typical demonstration of low-power-charging LEDs, we further illustrated their high-temperature sustainable lightening application in the study of high-power w-LED. The illuminance of w-LED containing HT-HPSs-6 gradually increased with increasing device current, while the constructed w-LED-based $CsPbBr_3$ could not be operated under a high forward-bias current (Figure 4d). Notably, our w-LED displays a superior durable high-power-driving capability, and its working current can go up to 300 mA, which is much higher than any previously reported materials (200 mA is the highest reported in the literature[11]). The illuminance of our LED device operating at such high power is sustainable and outstanding even the virtual chip temperature has gone beyond higher than 80 °C (Figure 4g). Thus, our w-LED seemingly can suppress the irreversible structural damage for the high charging electric current accompanied by higher operating temperatures. The device performance is much superior to the reported results of conventional rare-earth phosphor-based and other available perovskite-based LEDs (Table S3, Supporting Information[1]), especially for a wider and higher thresholder operating current range (20–300 mA) and longer working hours.

In summary, highly emissive and superb thermotolerant metal halide perovskite solid is successfully accomplished for the first time via a straightforward heterogeneous interfacial reaction. Our method overcomes the key problems (poor temperature tolerance and suboptimal quantum yield) in all existing perovskite solid synthesis methods. Since the ligand modification and Cs_4PbBr_6 hybrid encapsulation enhance the interaction between ligands and perovskite solid, our optimal perovskite solid can well maintain their superior quantum efficiency at the temperature over 150 °C for up to 22 h. Moreover, we demonstrated their use as long-lasting high-temperature and high-input-power durable solid-state light-emitting diodes. Such halide perovskites solid constructed LED exhibit high-temperature sustainability over 1100 h, which is three orders of magnitude longer compared to a LED constructed by metal halide perovskites solids ($CsPbBr_3$ solid) synthesized by conventional methods. In addition, the successful operation of a LED at 300 mA current density in our study also represents a significant

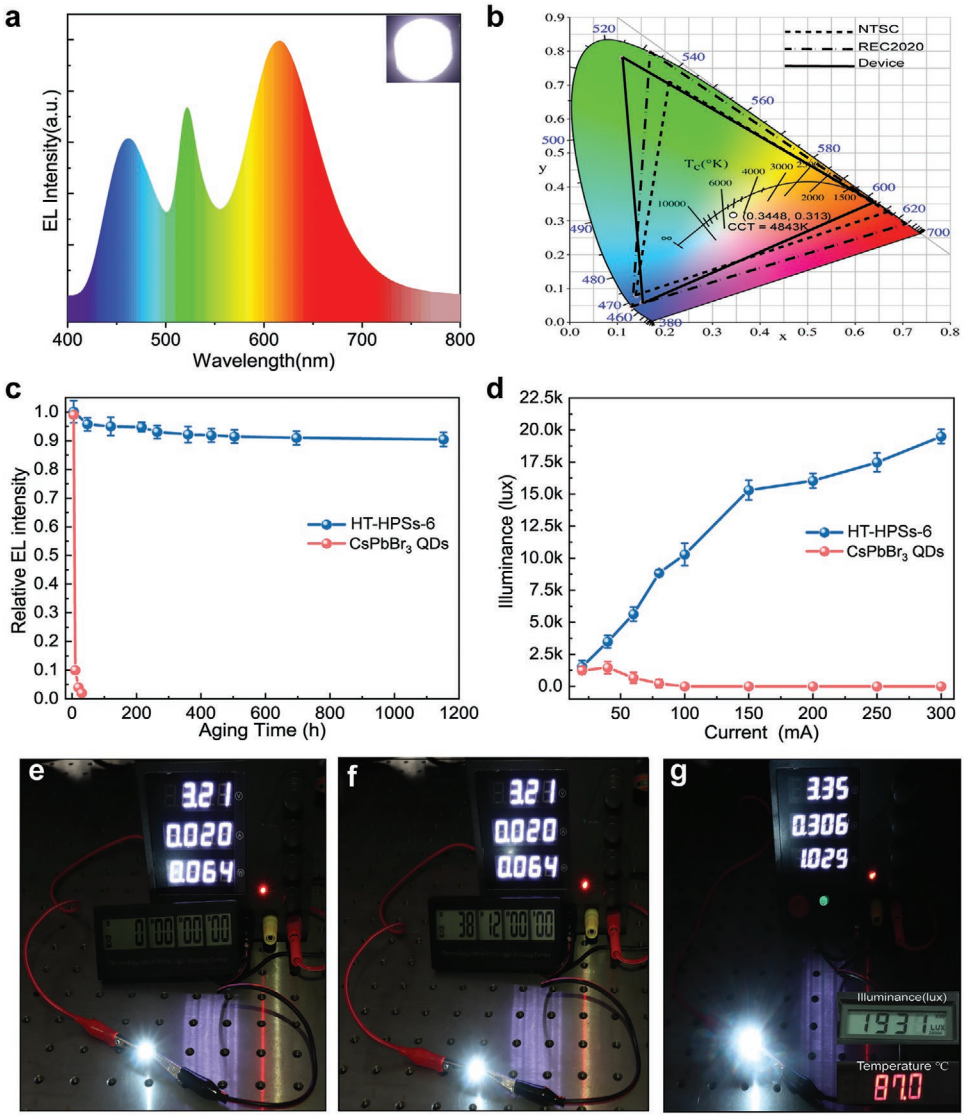

Figure 4. EL performance of the devices. a) EL spectra of the w-LED device. b) CIE color coordinates of the w-LED containing HT-HPSs-6 (thick solid triangle), NTCS (dotted triangle), and REC2020 standard (dashed triangle). c) Long-term operation of the perovskite-based devices at 20 mA for 1100 h. d) The illuminance of the w-LED as a function of forward-bias currents. e,f) Photographs of the w-LED operating at 20 mA for long-term operation. g) w-LED driven at a 300 mA forward current.

advance for high-power solid-state lighting. Such highly emissive and thermotolerant metal halide perovskites should set the stage for a wide array of solid-state lighting, lasing and display devices that have been limited by existing approaches.

Supporting Information

Supporting Information is available from the Wiley Online Library or from the author.

Acknowledgements

This work was financially supported by the National Natural Science Foundation of China (Grant No. 51602063), Guangdong Natural Science Foundation (Grant No. 2019A030310444), and Science and Technology Program of Guangzhou (Grant No. 201804010257). This work was also supported by Guangdong High-Level Personnel of Special Support Program and Open Fund of the State Key Laboratory of Luminescent Materials and Devices (South China University of Technology). This research was also supported by Major Program for Cooperative Innovation of Production, Education & Research of Guangzhou City (201704030106), and Special Fund for Application, Science and Technology Planning Projects of Guangdong Province of China (2017B010127002). G.H and K.H were supported by the startup fund of University of Massachusetts.

Conflict of Interest

The authors declare no conflict of interest.

Keywords

enhanced stability, heterogeneous interfacial method, solid-state metal halide perovskites, superior thermotolerance

Received: April 12, 2020
Published online:

[1] a) G. Li, T. Fleetham, E. Turner, X.-C. Hang, J. Li, *Adv. Opt. Mater.* **2015**, *3*, 390; b) X. Li, F. Cao, D. Yu, J. Chen, Z. Sun, Y. Shen, Y. Zhu, L. Wang, Y. Wei, Y. Wu, H. Zeng, *Small* **2017**, *13*, 1603996; c) H. Shao, X. Bai, G. Pan, H. Cui, J. Zhu, Y. Zhai, J. Liu, B. Dong, L. Xu, H. Song, *Nanotechnology* **2018**, *29*, 285706; d) Y. Wei, Z. Cheng, J. Lin, *Chem. Soc. Rev.* **2019**, *48*, 310; e) J. Xing, Y. Zhao, M. Askerka, L. N. Quan, X. Gong, W. Zhao, J. Zhao, H. Tan, G. Long, L. Gao, Z. Yang, O. Voznyy, J. Tang, Z.-H. Lu, Q. Xiong, E. H. Sargent, *Nat. Commun.* **2018**, *9*, 3541; f) G. Li, F. W. R. Rivarola, N. J. L. K. Davis, S. Bai, T. C. Jellicoe, F. de la Peña, S. Hou, C. Ducati, F. Gao, R. H. Friend, N. C. Greenham, Z.-K. Tan, *Adv. Mater.* **2016**, *28*, 3528; g) H. Lu, Y. Tang, L. Rao, Z. Li, X. Ding, C. Song, B. Yu, *Nanotechnology* **2019**, *30*, 295603.

[2] a) X. He, Y. Qiu, S. Yang, *Adv. Mater.* **2017**, *29*, 1700775; b) T. Leijtens, K. A. Bush, R. Prasanna, M. D. McGehee, *Nat. Energy* **2018**, *3*, 828; c) C. Liu, W. Li, C. Zhang, Y. Ma, J. Fan, Y. Mai, *J. Am. Chem. Soc.* **2018**, *140*, 3825.

[3] a) N. J. Jeon, J. H. Noh, W. S. Yang, Y. C. Kim, S. Ryu, J. Seo, S. I. Seok, *Nature* **2015**, *517*, 476; b) P. Jiang, Y. Peng, Y. Mou, H. Cheng, M. Chen, S. Liu, *Appl. Opt.* **2017**, *56*, 7921; c) R. Prasanna, T. Leijtens, S. P. Dunfield, J. A. Raiford, E. J. Wolf, S. A. Swifter, J. Werner, G. E. Eperon, C. de Paula, A. F. Palmstrom, C. C. Boyd, M. F. A. M. van Hest, S. F. Bent, G. Teeter, J. J. Berry, M. D. McGehee, *Nat. Energy* **2019**, *4*, 939; d) P. Pust, V. Weiler, C. Hecht, A. Tücks, A. S. Wochnik, A.-K. Henß, D. Wiechert, C. Scheu, P. J. Schmidt, W. Schnick, *Nat. Mater.* **2014**, *13*, 891; e) Z. Yang, Z. Yu, H. Wei, X. Xiao, Z. Ni, B. Chen, Y. Deng, S. N. Habisreutinger, X. Chen, K. Wang, J. Zhao, P. N. Rudd, J. J. Berry, M. C. Beard, J. Huang, *Nat. Commun.* **2019**, *10*, 4498.

[4] a) L. Lv, Y. Xu, H. Fang, W. Luo, F. Xu, L. Liu, B. Wang, X. Zhang, D. Yang, W. Hu, A. Dong, *Nanoscale* **2016**, *8*, 13589; b) S. A. Veldhuis, P. P. Boix, N. Yantara, M. Li, T. C. Sum, N. Mathews, S. G. Mhaisalkar, *Adv. Mater.* **2016**, *28*, 6804; c) P. Brenner, O. Bar-On, M. Jakoby, I. Allegro, B. S. Richards, U. W. Paetzold, I. A. Howard, J. Scheuer, U. Lemmer, *Nat. Commun.* **2019**, *10*, 988.

[5] a) D. Chen, Z. Wan, X. Chen, Y. Yuan, J. Zhong, *J. Mater. Chem. C* **2016**, *4*, 10646; b) Y.-M. Chen, Y. Zhou, Q. Zhao, J.-Y. Zhang, J.-P. Ma, T.-T. Xuan, S.-Q. Guo, Z.-J. Yong, J. Wang, Y. Kuroiwa, C. Moriyoshi, H.-T. Sun, *ACS Appl. Mater. Interfaces* **2018**, *10*, 15905.

[6] a) Y. Fu, H. Zhu, C. C. Stoumpos, Q. Ding, J. Wang, M. G. Kanatzidis, X. Zhu, S. Jin, *ACS Nano* **2016**, *10*, 7963; b) K. Wang, S. Wang, S. Xiao, Q. Song, *Adv. Opt. Mater.* **2018**, *6*, 1800278; c) S. Yakunin, L. Protesescu, F. Krieg, M. I. Bodnarchuk, G. Nedelcu, M. Humer, G. De Luca, M. Fiebig, W. Heiss, M. V. Kovalenko, *Nat. Commun.* **2015**, *6*, 8056.

[7] a) L. K. Bharat, S.-K. Jeon, K. G. Krishna, J. S. Yu, *Sci. Rep.* **2017**, *7*, 42348; b) I. A. Mir, V. S. Radhakrishanan, K. Rawat, T. Prasad, H. B. Bohidar, *Sci. Rep.* **2018**, *8*, 9322; c) X. Zhen, Y. Tao, Z. An, P. Chen, C. Xu, R. Chen, W. Huang, K. Pu, *Adv. Mater.* **2017**, *29*, 1606665; d) G. Li, H. Wang, T. Zhang, L. Mi, Y. Zhang, Z. Zhang, W. Zhang, Y. Jiang, *Adv. Funct. Mater.* **2016**, *26*, 8478.

[8] X. Li, Y. Wu, S. Zhang, B. Cai, Y. Gu, J. Song, H. Zeng, *Adv. Funct. Mater.* **2016**, *26*, 2435.

[9] a) S. Huang, Z. Li, B. Wang, N. Zhu, C. Zhang, L. Kong, Q. Zhang, A. Shan, L. Li, *ACS Appl. Mater. Interfaces* **2017**, *9*, 7249; b) M. I. Saidaminov, J. Almutlaq, S. Sarmah, I. Dursun, A. A. Zhumekenov, R. Begum, J. Pan, N. Cho, O. F. Mohammed, O. M. Bakr, *ACS Energy Lett.* **2016**, *1*, 840.

[10] a) A. Dey, P. Rathod, D. Kabra, *Adv. Opt. Mater.* **2018**, *6*, 1800109; b) F. Krieg, S. T. Ochsenbein, S. Yakunin, S. ten Brinck, P. Aellen, A. Süess, B. Clerc, D. Guggisberg, O. Nazarenko, Y. Shynkarenko, S. Kumar, C.-J. Shih, I. Infante, M. V. Kovalenko, *ACS Energy Lett.* **2018**, *3*, 641; c) Q. Wang, W. Wu, R. Wu, S. Yang, Y. Wang, J. Wang, Z. Chai, Q. Han, *J. Colloid Interface Sci.* **2019**, *554*, 133.

[11] X. Chen, F. Zhang, Y. Ge, L. Shi, S. Huang, J. Tang, Z. Lv, L. Zhang, B. Zou, H. Zhong, *Adv. Funct. Mater.* **2018**, *28*, 1706567.

[12] W. Wang, D. Wang, F. Fang, S. Wang, G. Xu, T. Zhang, *Cryst. Growth Des.* **2018**, *18*, 6133.

[13] a) T. Xuan, S. Lou, J. Huang, L. Cao, X. Yang, H. Li, J. Wang, *Nanoscale* **2018**, *10*, 9840; b) Y. Zhang, M. I. Saidaminov, I. Dursun, H. Yang, B. Murali, E. Alarousu, E. Yengel, B. A. Alshankiti, O. M. Bakr, O. F. Mohammed, *J. Phys. Chem. Lett.* **2017**, *8*, 961.

[14] a) S. Lou, T. Xuan, Q. Liang, J. Huang, L. Cao, C. Yu, M. Cao, C. Xia, J. Wang, D. Zhang, H. Li, *J. Colloid Interface Sci.* **2019**, *537*, 384; b) A. Swarnkar, R. Chulliyil, V. K. Ravi, M. Irfanullah, A. Chowdhury, A. Nag, *Angew. Chem., Int. Ed.* **2015**, *54*, 15424; c) Q. Zhong, M. Cao, H. Hu, D. Yang, M. Chen, P. Li, L. Wu, Q. Zhang, *ACS Nano* **2018**, *12*, 8579.

[15] L. N. Quan, R. Quintero-Bermudez, O. Voznyy, G. Walters, A. Jain, J. Z. Fan, X. Zheng, Z. Yang, E. H. Sargent, *Adv. Mater.* **2017**, *29*, 1605945.

[16] D. Yan, T. Shi, Z. Zang, T. Zhou, Z. Liu, Z. Zhang, J. Du, Y. Leng, X. Tang, *Small* **2019**, *15*, 1901173.

[17] J. Shamsi, A. L. Abdelhady, S. Accornero, M. Arciniegas, L. Goldoni, A. R. S. Kandada, A. Petrozza, L. Manna, *ACS Energy Lett.* **2016**, *1*, 1042.

[18] H. Zhang, Q. Liao, Y. Wu, J. Chen, Q. Gao, H. Fu, *Phys. Chem. Chem. Phys.* **2017**, *19*, 29092.

[19] Z. Dang, B. Dhanabalan, A. Castelli, R. Dhall, K. C. Bustillo, D. Marchelli, D. Spirito, U. Petralanda, J. Shamsi, L. Manna, R. Krahne, M. P. Arciniegas, *Nano Lett.* **2020**, *20*, 1808.

[20] a) J. Li, L. Xu, T. Wang, J. Song, J. Chen, J. Xue, Y. Dong, B. Cai, Q. Shan, B. Han, H. Zeng, *Adv. Mater.* **2017**, *29*, 1603885; b) D. Yang, X. Li, W. Zhou, S. Zhang, C. Meng, Y. Wu, Y. Wang, H. Zeng, *Adv. Mater.* **2019**, *31*, 1900767.

[21] M. Su, B. Fan, H. Li, K. Wang, Z. Luo, *Nanoscale* **2019**, *11*, 1335.

[22] a) R. Cao, L. Wu, X. Di, P. Li, G. Hu, X. Liang, W. Xiang, *Opt. Mater.* **2017**, *70*, 92; b) L. Huang, Y. Liu, J. Yu, Y. Zhu, F. Pan, T. Xuan, M. G. Brik, C. Wang, J. Wang, *ACS Appl. Mater. Interfaces* **2018**, *10*, 18082; c) S. Li, L. Wang, D. Tang, Y. Cho, X. Liu, X. Zhou, L. Lu, L. Zhang, T. Takeda, N. Hirosaki, R.-J. Xie, *Chem. Mater.* **2018**, *30*, 494.

[23] M. Zhao, H. X. Liao, L. X. Ning, Q. Y. Zhang, Q. L. Liu, Z. G. Xia, *Adv. Mater.* **2018**, *30*, 1802489.